Acta Biomaterialia 9 (2013) 7937–7947

Contents lists available at SciVerse ScienceDirect

Acta Biomaterialia

journal homepage: www.elsevier.com/locate/actabiomat

Multiscale modelling and diffraction-based characterization of elastic behaviour of human dentine

Tan Sui [a,*], Michael A. Sandholzer [b], Nikolaos Baimpas [a], Igor P. Dolbnya [c], Anthony Damien Walmsley [b], Philip J. Lumley [b], Gabriel Landini [b], Alexander M. Korsunsky [a]

[a] Department of Engineering Science, University of Oxford, Parks Road, Oxford OX1 3PJ, UK
[b] School of Dentistry, College of Medical and Dental Sciences, University of Birmingham, St. Chad's Queensway, Birmingham B4 6NN, UK
[c] Beamline B16, Diamond Light Source, Harwell Oxford Campus, Didcot OX11 0DE, UK

ARTICLE INFO

Article history:
Received 23 November 2012
Received in revised form 10 April 2013
Accepted 11 April 2013
Available online 18 April 2013

Keywords:
Dentine
WAXS/SAXS
Eshelby model
Mechanical properties

ABSTRACT

Human dentine is a hierarchical mineralized tissue with a two-level composite structure, with tubules being the prominent structural feature at a microlevel, and collagen fibres decorated with hydroxyapatite (HAp) crystallite platelets dominating the nanoscale. Few studies have focused on this two-level structure of human dentine, where the response to mechanical loading is thought to be affected not only by the tubule volume fraction at the microscale, but also by the shape and orientation distribution of mineral crystallites, and their nanoscale spatial arrangement and alignment. In this paper, in situ elastic strain evolution within HAp in dentine subjected to uniaxial compressive loading along both longitudinal and transverse directions was characterized simultaneously by two synchrotron X-ray scattering techniques: small- and wide-angle X-ray scattering (SAXS and WAXS, respectively). WAXS allows the evaluation of the apparent modulus linking the external load to the internal HAp crystallite strain, while the nanoscale HAp distribution and arrangement can be quantified by SAXS. We proposed an improved multiscale Eshelby inclusion model that takes into account the two-level hierarchical structure, and validated it with a multidirectional experimental strain evaluation. The agreement between the simulation and measurement indicates that the multiscale hierarchical model developed here accurately reflects the structural arrangement and mechanical response of human dentine. This study benefits the comprehensive understanding of the mechanical behaviour of hierarchical biomaterials. The knowledge of the mechanical properties related to the hierarchical structure is essential for the understanding and predicting the effects of structural alterations that may occur due to disease or treatment on the performance of dental tissues and their artificial replacements.

1. Introduction

Dentine is a hydrated biological mineral composite tissue with a hierarchical structure and versatile mechanical properties [1]. At the microscopic level, dentine has a well-oriented structure with an arrangement of dentinal tubules that extend throughout the entire dentine thickness, from the amelo-dentinal junction (ADJ) to the pulp [1–3]. At the nanoscale, dentine is a composite of platelike hydroxyapatite crystals (HAp) that have the shape of elongated pancakes (~2–4 nm thick, ~30 nm wide and up to 100 nm long) randomly embedded in a collagen matrix [4,5]. Characterizing the mechanical properties of the tissue according to its complex hierarchical structure benefits the understanding of the internal architecture and hierarchical properties of materials.

Previously, most research in this area has concentrated on the mechanical properties of dentine at the macro- and microscale, i.e. Young's modulus, Poisson's ratio, hardness and fracture properties, using a variety of measurement methods [6]. However, few studies have focused on the nanoscale, where mechanical alterations can be considered to be a function of crystal shape and orientation of the mineral phase [7,8]. During elastic loading, stresses are expected to be transferred to the stiff HAp platelets from the surrounding collagen matrix [7]. To investigate this, it is required to use techniques that allow in situ quantification of the mechanical response of nanoscale HAp phases to loading.

Synchrotron-based X-ray diffraction, and small- and wide-angle X-ray scattering (SAXS and WAXS, respectively), are advanced nondestructive techniques that enable characterization of the nanoscale and subnanoscale structure of materials, and have been widely used to study load transfer between two phases in matrix composites [9–11]. In situ compression testing, in combination with the WAXS technique, has been used to quantify the internal strains of

* Corresponding author. Tel.: +44 18652 83447; fax: +44 18652 73010.
E-mail address: tan.sui@eng.ox.ac.uk (T. Sui).

1742-7061/$ - see front matter © 2013 Acta Materialia Inc. Published by Elsevier Ltd. All rights reserved.
http://dx.doi.org/10.1016/j.actbio.2013.04.020

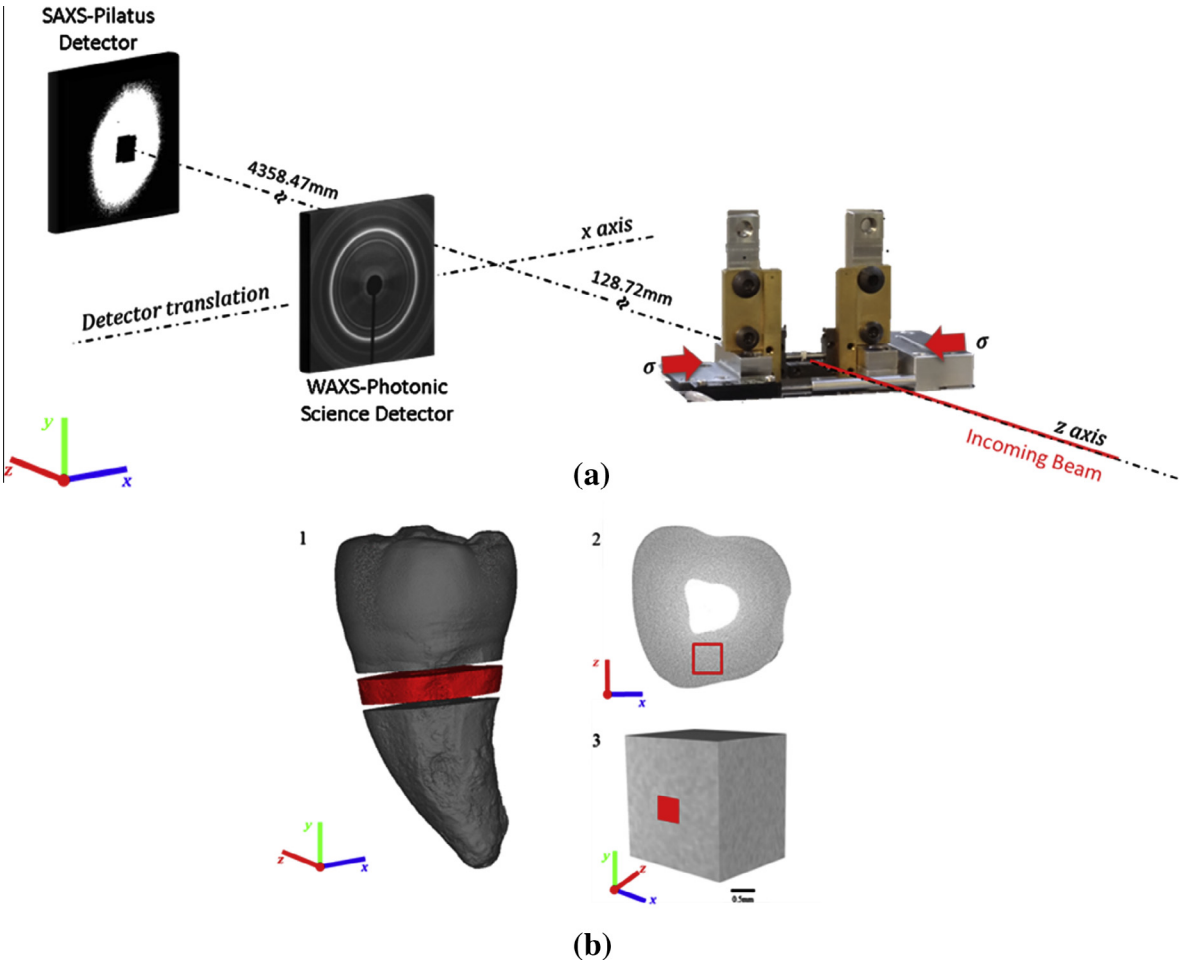

Fig. 1. Schematic diagram of experimental setup and sample preparation. (a) Sample under uniaxial compressive loading on the compression stage. The monochromatic X-ray beam was directed perpendicular to the sample surface and the loading direction. WAXS and SAXS diffraction patterns were recorded at each loading step at three locations on the sample. The WAXS detector was translated laterally out of the beam to expose the SAXS detector after each collection of WAXS. (b) Micro-CT-based models of the three preparation stages. (1) 2 mm thick dentine disk (coloured red) cut below the enamel–cement line and (2) further cut and polished to produce (3) the final 2 mm × 2 mm × 2 mm cubes of dentine. The red square indicates the central position of the X-ray beam.

the phase [9–11]. In addition, for mineralized tissues, SAXS is able to reveal quantitative nanoscale information about the structure, orientation and degree of alignment of crystals [12]. Those parameters have been identified as critical for the mechanical properties and stability of the materials [13–15]. It is only recently that this technique has been applied to the study of mechanical behaviour in mineralized biological composites such as bone [16–19] and teeth [7,8,20]. Deymier-Black et al. [7] determined the longitudinal apparent modulus of HAp in bovine dentine using synchrotron-based WAXS, while strain distribution across the ADJ in bovine teeth was investigated by Almer and Stock [20]. A deep understanding of the relationship between the nanoscale structure and macroscopic mechanical behaviour is lacking. Earlier studies do not take into account the nanoparticle distribution [7,20], which can be derived from SAXS data. In addition, all these studies were carried on non-human samples, in which different particularities of the tubule structure and morphology are expected to result in differences in the mechanical properties [21].

In parallel, various analytical models of composites have been proposed to describe the interaction of different mineral phases and model the elastic properties of hard tissues (e.g. [22–24]). Besides these, one widely accepted model is the Eshelby inclusion model [25,26]. Recently, the Eshelby model has also been applied in dental research based on nanoindentation and finite-element model data [27–30] to explain and predict the elastic response of dentine on the microscopic level. However, the models used in previous simulations were limited, in which no consideration was given to the nanoscale structure, and this led to discrepancies of overestimation between the predictions and experimental results [7].

In order to improve the understanding of the influence of the nanoscale structure variation of the two-level composite of human dentine on its mechanical response, in this study, the in situ synchrotron X-ray techniques (simultaneous SAXS/WAXS) were used to measure the elastic strain (WAXS), alterations in crystal orientation and degree of alignment of HAp phases (SAXS) in human dentine under externally uniaxial compressive loading along two directions, longitudinal as well as transverse with respect to the preferential tubule direction. Meanwhile, an extended multiscale Eshelby model for a two-level composite was established. The capability of the model in capturing the relationship between the nanoscale structure and macroscopic loading was evaluated.

2. Materials and methods

2.1. Sample preparation

Two freshly extracted sound human third molars (ethical approval obtained from the National Research Ethics Committee; NHS-REC reference 09.H0405.33/Consortium R&D No. 1465) were

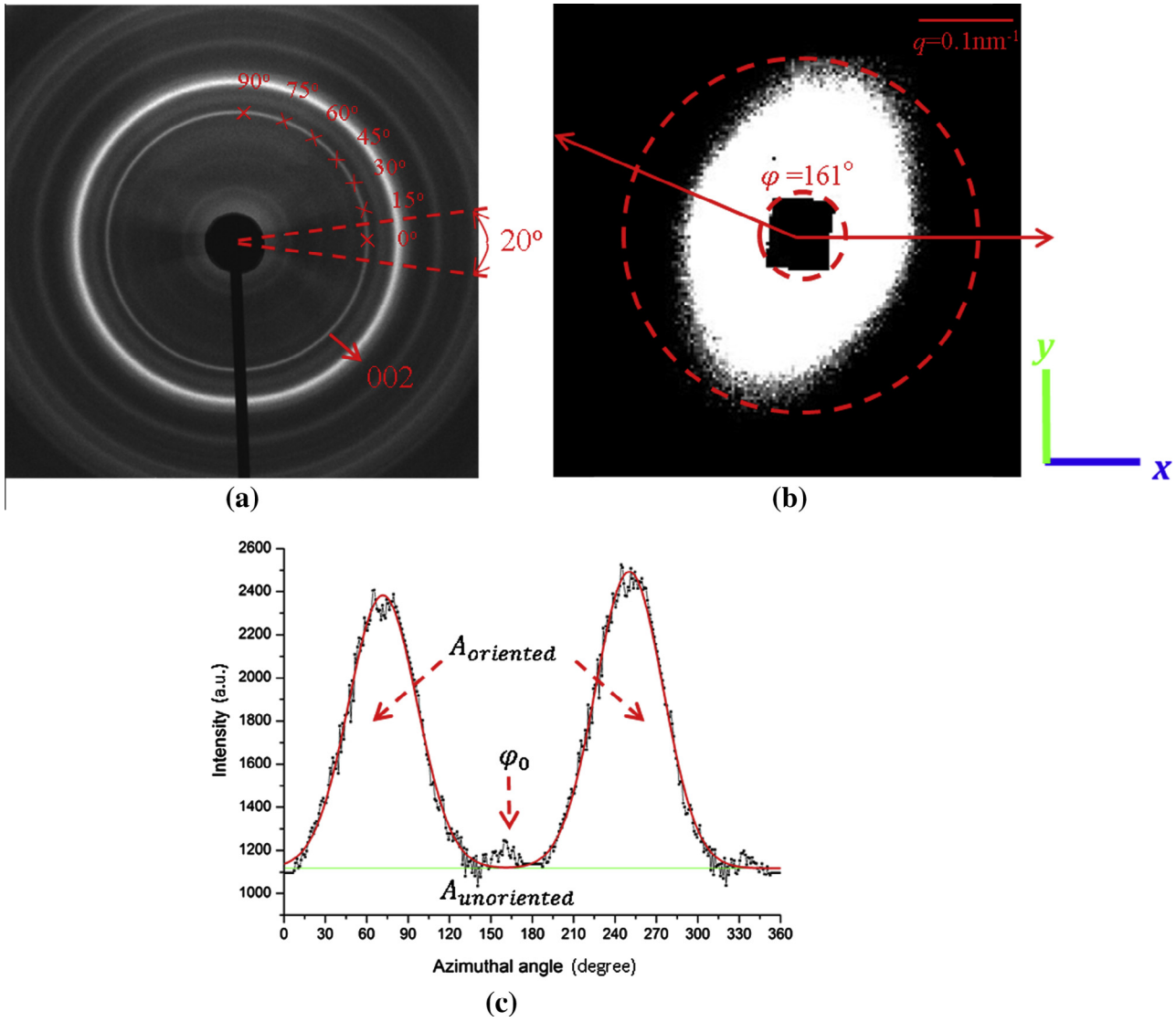

Fig. 2. (a) A representative dentine WAXS pattern of Debye–Scherrer rings with different intensities. The dark region in the centre is the beam stop. The (002) peak is marked with a red arrow. Peak shifts at different positions on the (002) ring represent the average strains of (002) along different directions. Multiple angles with respect to the x-axis were caked in order to examine the strain variation (seven angles are shown as an example: 0°, 15°, 30°, 45°, 60°, 75°, 90°). Each cake was with a 20° range. (b) A representative dentine SAXS pattern of the HD2 sample. The q scale in the SAXS pattern is in reciprocal space, which is the inverse of d dimension in the real space. The relation is $q = 2\pi/d$. If all the HAp platelets are oriented in the φ direction parallel to their long dimension in the real space, q would be the smallest in the elliptical pattern of the SAXS. Thus the direction of the short axis of the ellipse pattern indicates the predominant orientation of the crystals. (c) A plot of $I(\varphi)$ of the HD2 sample without any external load (black points). The Gauss fit is also shown in the figure (red line). The predominant orientation $\varphi_0 = 161^\circ$ is the average position of the two peaks. The ratio $A_{oriented}/(A_{oriented} + A_{unoriented})$ gives the degree of alignment.

washed and cleaned in distilled water to eliminate residues and kept in a −20 °C freezer for a maximum of 14 days before the experiment. The samples were rehydrated using distilled water and 2 mm thick dentine disks were cut just below the enamel–cement line using a low-speed diamond saw (Isomet Buehler Ltd., Lake Bluff, IL, USA). The disks were further cut into smaller bars and a series of polishing papers was used to produce the final 2 mm × 2 mm × 2 mm cubes of dentine (Fig. 1b). The samples were kept for a maximum of 7 days in distilled water in a commercial fridge at 4 °C until the experiment was performed.

2.2. In situ scattering measurements

2.2.1. Mechanical loading setup

Uniaxial compressive loading was carried out on two dentine samples in the form of small 2 mm × 2 mm × 2 mm cubes. The samples were designated HD2, for which the loading was applied in the transverse direction, and HD3, for which the loading was applied in the longitudinal direction with respect to the tubules, respectively. Loading was carried out using a remotely operated and monitored compression rig (Deben, Suffolk, UK), with a 5 kN calibrated load cell. The rig was equipped with custom-made jaws, allowing a high-energy transmission X-ray setup to be used, as illustrated in Fig. 1a. The samples were deformed at a displacement rate of 0.2 mm min^{-1} up to 400 N (corresponding to ~100 MPa for the samples) along the x-direction. After each constant loading increments (HD2 50 N, HD3 100 N), the load was maintained and the WAXS and SAXS patterns were collected.

2.2.2. Beamline diffraction setup

The experiment was carried out on B16 experimental beamline at Diamond Light Source, Oxford Harwell Campus, Didcot, UK. A

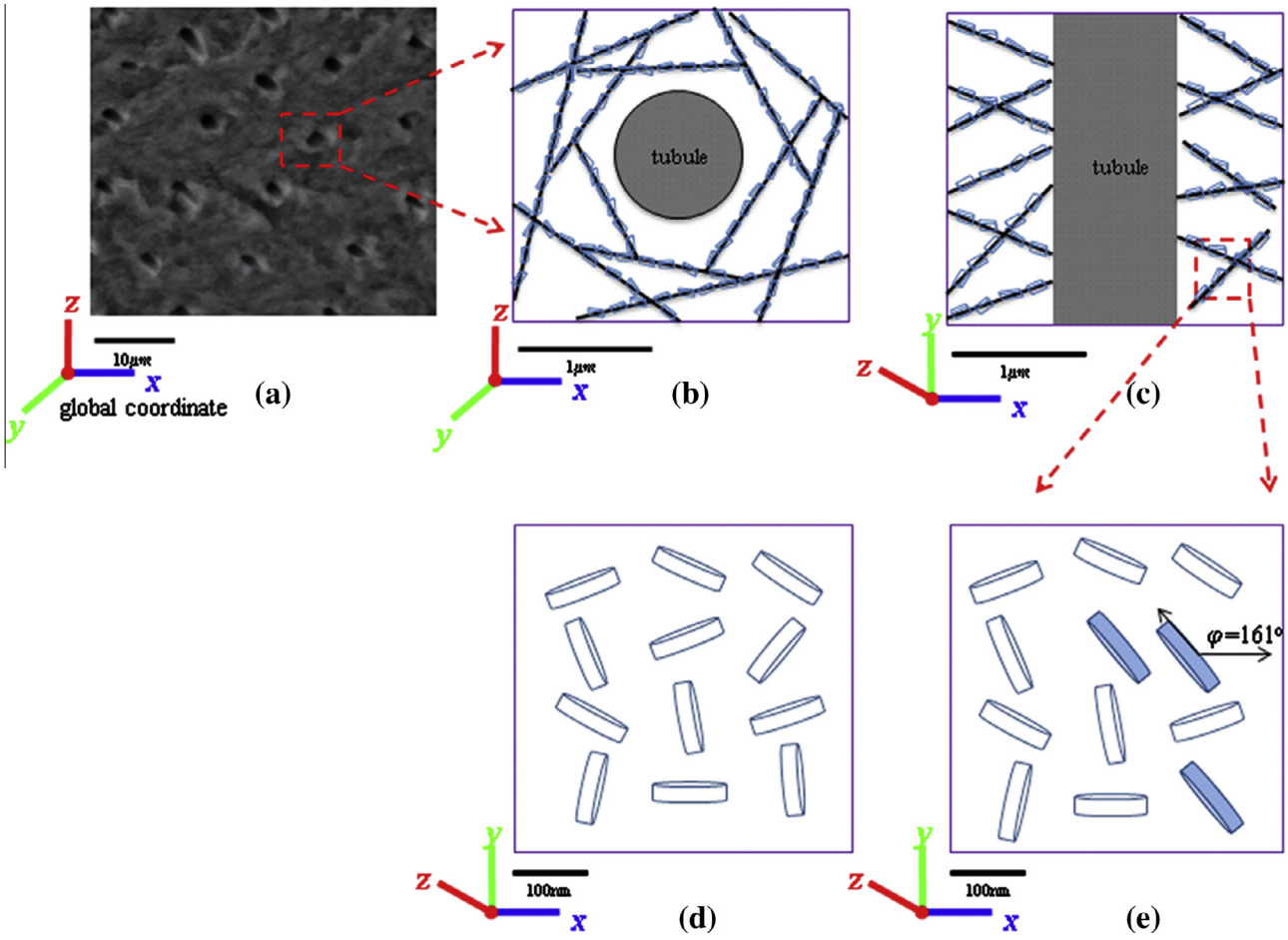

Fig. 3. (a) SEM observation of the first-level tubule structure of human dentine. (b) A schematic structure of the random distribution of collagen fibrils (black lines) beside the tubules, viewed along the longitudinal direction of tubules. (c) Same as (b), viewed along the transverse direction of tubules. (d) The structure of the random distribution of HAp crystals viewed from the cross-section parallel to the tubule direction. (e) The real structure of partial alignment, where the pennies having an alignment angle 161° (showing the example of HD2) with respect to the global x-axis are shown in blue.

monochromatic X-ray beam was used to illuminate the sample as illustrated schematically in Fig. 1a. The incident beam was monochromated to the photon energy of 17.99 keV, and collimated to the spot size of 0.5 mm × 0.5 mm on the sample. WAXS and SAXS patterns were alternately collected at three locations across the sample. A silicon powder was used for the WAXS data calibration and dry chicken collagen was used for the SAXS data calibration [31].

WAXS diffraction patterns were recorded using a Photonic Science Image Star 9000 detector (Photonic Science Ltd., UK) placed at a sample-to-camera distance of 128.72 mm (Fig. 1a). Further downstream of the beam a Pilatus 300K detector (Dectris, Baden, Switzerland) was positioned at a distance of 4358.47 mm to collect the SAXS patterns (Fig. 1a). In order to record both the WAXS and SAXS patterns at each scanning location, the WAXS detector was translated laterally to expose the SAXS detector after each WAXS collection.

2.3. Micro-CT protocol and data processing

For the purpose of planning the measuring positions and determination of the precise loading cross-sectional area of the dentine cubes, a commercial micro-computed tomography (micro-CT) system was used to scan the samples with a SkyScan 1172 scanner (SkyScan, Kontich, Belgium) at 1.9 μm isotropic resolution using 40 kV voltage, 120 μA current and a 0.5 mm Al filter. The resulting slices were reconstructed with the SkyScan NRECON package and subsequent 3-D planning models were created with Fiji imaging software [32].

2.4. Scattering data analysis

2.4.1. WAXS data analysis

The data analysis was done in accordance with previous studies [9–11]. The WAXS data interpretation was limited to the (002) peak of Debye–Scherrer rings of the middle scanning location (see Fig. 2a), guaranteeing that the same position could be detected during the compressive deformation of the dentine. Changes in the d-spacing between the lattice planes in the HAp were used to determine the elastic strain in the mineral HAp phase [33]. The apparent lattice elastic strain ε was computed from the definition:

$$\varepsilon = \frac{d_{002} - d^0_{002}}{d^0_{002}}, \tag{1}$$

where d_{002} is the apparent strained d-spacing and d^0_{002} is the reference strain-free value of the d-spacing.

To determine the strain from the mineral HAp phase, 2-D diffraction images were pre-processed into a 1-D intensity plot using Fit2D [34] by "caking" (a professional jargon term used to refer to the selection of a sector in the radial–azimuthal coordinates of each pattern) each pattern with a step of 20° in the range of 0°–360° of the (002) peak under laboratory coordinates (Fig. 2a, only

Table 1
Experimental results from SAXS/WAXS and refined parameters in the Eshelby model of the two dentine samples.

Parameters	HD2_value	HD3_value	Reference values
Orientation (degree)	161	78	
Degree of alignment	0.289	0.168	
K_exp. (GPa)	22.129	24.156	
f_1	10%	10%	3.6 – 10.2% [45]
f_2	40%	38%	30.5%, 44.4% [46]
$C_{M1} = C_{M2}$	E_m = 1.1 GPa, υ_m = 0.3	E_m = 0.8 GPa, υ_m = 0.27	$E_{collagen}$ = 1 GPa, $\upsilon_{collagen}$ = 0.30 [27]
C_{HAp}	E_{HAp} = 90 GPa, υ_{HAp} = 0.32	E_{HAp} = 90 GPa, υ_{HAp} = 0.32	E_{HAp} = 40–117 GPa, υ_{HAp} = 0.27 [47]
a_1/a_3	31	31	(2–4) × 30 × 100 nm^3[4,5]
K_model (GPa)	22.870	24.189	

0°–90° is shown). The normal strain component along the centre direction of each cake represents the strain distribution at the corresponding orientation. Subsequently, the 1-D intensity plot of each cake (covering 20°) was obtained by the integration, with respect to the azimuthal angle, of the converted 2-D images. Afterwards, the 1-D profiles of each individual (002) peak was fitted with Gaussian curves to determine the centre position after the subtraction of the linearly fitted background. To calculate the HAp lattice strain, the WAXS pattern of the unloaded condition was used as a strain-free reference point.

2.4.2. SAXS data analysis

For the SAXS data analysis, a reference pattern representing the strain-free sample was used to determine the orientation and degree of alignment (ρ) of HAp crystalline particles, which describes the percentage of aligned particles. Fig. 2b is an example reference SAXS pattern of HD2. In order to quantify the orientation and degree of alignment, the SAXS patterns were integrated along all the possible scattering vectors q to account for the main scattering effect (with the range selected from the outline of beamstop to the outline of the pattern as marked with red dashes in Fig. 2b), which results in a function $I(\varphi)$ with the azimuthal angle φ [35–37] (Fig. 2c). The predominant orientation is determined by the average position of two peaks in the plot of $I(\varphi)$ (e.g. φ_0 in Fig. 2c), while the degree of alignment with respect to the predominant orientation of HAp is defined as the ratio of peak area and the overall area under the curve of $I(\varphi)$:

$$\rho = \frac{A_{oriented}}{A_{oriented} + A_{unoriented}}, \tag{2}$$

where $A_{unoriented}$ is the area of the constant background level and $A_{oriented}$ depicts the total area subtracting the background. The value of degree of alignment ranges from 0 to 1, where $\rho = 0$ indicates no predominant orientation within the plane of the section and $\rho = 1$ indicates a perfect alignment of all crystals [35,37].

3. Model formulation

3.1. Geometrical assumptions

Human dentine has a hierarchical two-level composite structure, where the first level is represented by the dentinal tubules and the second level by the HAp crystals within a fibrous collagen matrix. Fig. 3a–c are images of the first-level dentine structure, where Fig. 3a is obtained by scanning electron microscopy (SEM) and Fig. 3b,c show the random distribution of collagen fibril viewed respectively along longitudinal and transverse direction of tubules as proposed by Bozec [38]. Fig. 3d,e are images of the second-level dentine structure, where a randomly distributed structure of HAp crystals shown in Fig. 3d is to be combined with a fully aligned structure to determine the real structure of partial alignment (Fig. 3e for HD2), given the detailed information of degree of alignment by SAXS interpretation. Both levels are non-dilute systems consisting of a number of inhomogeneous inclusions. The multiscale Eshelby model for a non-dilute system is established and is used here to model the two-level composite of dentine [39] (for details see Appendix). The first-level model regards the whole dentine sample as composed of aligned tubules within a matrix phase, while the second-level model considers the matrix of the first level as a composite in detail, consisting of HAp crystals and a collagen matrix.

The shape of the HAp crystalline platelets in dentine is thought to correspond to elongated flagstone. In classical Eshelby modelling, a very good approximation is to use a penny-shape inclusion to simulate an individual platelet, as the integrals can be readily written. The Eshelby penny-shaped tensor has two parameters, where a_1 is the radius while a_3 is half of the thickness of the penny-shaped inclusion [40]. The thickness of the penny-shape is taken to be equal to the thickness of the dentine crystal platelet (2–4 nm). The diameter of the penny-shape is the average of the length (100 nm) and width (30 nm) of HAp to guarantee the identical cross-sectional area. The size of crystal platelet and the parameters of penny-shape tensor are listed in Table 1. The crystal c-axis (corresponding to the (002) peak) of the HAp crystallites is thought to be parallel to the long dimension of the platelet [41,42]. Therefore, in the model, the c-axis lies along the radial direction within the penny and is in the x–y plane shown in Fig. 3e.

3.2. First-level model: multiple aligned tubule inclusions within dentine matrix

The purpose of the first-level model for human dentine is to establish the elastic relationship between the external stress σ^A and dentine matrix stress σ_{M1}, which will serve as the external stress in the second level. Without any transformation strain in tubules, the Eshelby model for a non-dilute system (Appendix Eqs. (B1), (B2), (B3), (B4), (B5)) indicates that the mechanical response of the tubules can be related to an equivalent inclusion with the same property as the matrix:

$$\langle C\rangle_{tubule}(\langle\varepsilon\rangle^i + \langle\varepsilon\rangle_{M1} + \varepsilon^A) = C_{M1}(\langle\varepsilon\rangle^i + \langle\varepsilon\rangle_{M1} + \varepsilon^A - \langle\varepsilon\rangle^t), \tag{3}$$

where "*M1*" means the first-level matrix, $\langle\varepsilon\rangle^i$ the average total strain in tubules, $\langle C\rangle_{tubule}$ the average stiffness matrix of tubules, $\varepsilon^A = C_{M1}\sigma^A$ the external strain, $C_{M1}\langle\varepsilon\rangle_{M1} = \langle\sigma\rangle_{M1}$ the "image" stress defined to satisfy the boundary conditions at the external surface of a finite composite [25,39] and $\langle\varepsilon\rangle^t$ is the average transformation strain in the equivalent inclusion to be determined. Considering that the average stiffness of tubules is null $\langle C\rangle_{tubule} = 0$, the average stress in the dentine first-level matrix can be expressed merely in terms of the volume fraction of tubules f_1 (for further details see Appendix, Eqs. ((B7), (B8), (B9), (B10)), [25,39]):

$$\sigma_{M1} = \sigma^A + \langle\sigma\rangle_{M1} = \frac{1}{1-f_1}\sigma^A. \tag{4}$$

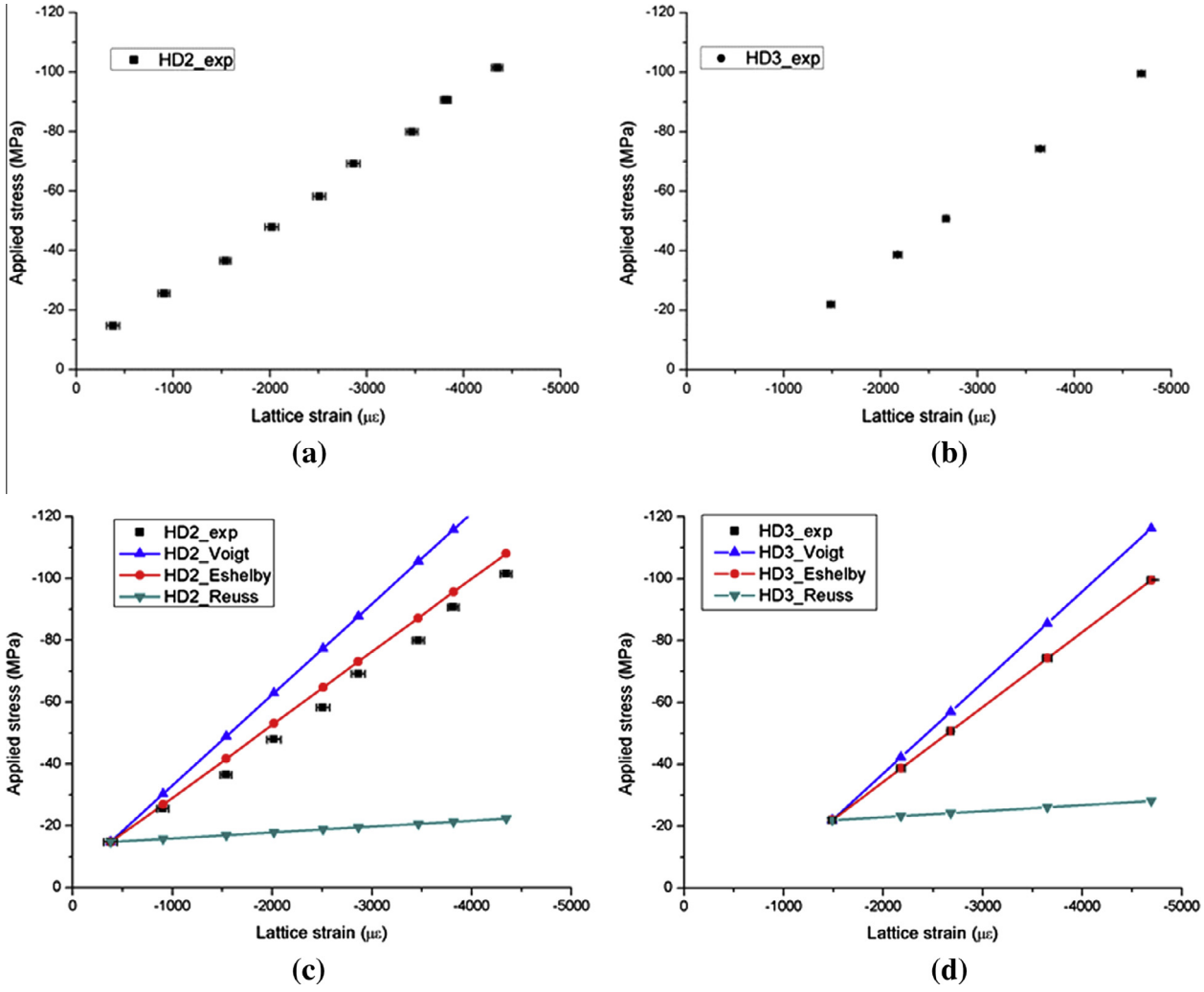

Fig. 4. Comparison of experimental data and modelling results of applied compressive stress vs. elastic lattice strain for HAp. (a) HD2 experimental data (error bar: 1 SD); (b) HD3 experimental data (error bar: 1 SD). (c) HD2 data (black points) and modelling results (red line: multiscale Eshelby model; blue line: Voigt bound; dark grey: Reuss bound) with the compressive stress along transverse direction with respect to the tubules. (d) HD3 data (black points) and modelling results (red line: multiscale Eshelby model; blue line: Voigt bound; dark grey: Reuss bound) with the compressive stress along longitudinal direction with respect to the tubules. The compressive stresses of HD2 and HD3 were uniformly selected under 100 MPa.

3.3. Second-level model: HAp inclusion of collagen matrix

The dispersion of multiple HAp crystals within the matrix of collagen forms the second hierarchical level model for dentine. The purpose of the second level model is to establish a relationship between the first-level dentine matrix stress and the average strain in the HAp crystals $\langle\varepsilon\rangle^{HAp}$, and thereby to determine the apparent modulus [43] between the global external load and local HAp crystal strain.

3.3.1. Multiple perfectly aligned HAp crystals

If all HAp crystals are perfectly aligned described by an orientation matrix T, the relationship between the average Hap crystal strain and the external load (here the first-level dentine matrix stress) can be expressed as [39] (Appendix Eq. (B11)):

$$\langle\varepsilon\rangle^{HAp}_{aligned} = \{\{(I - C_{M2}^{-1}\langle C\rangle_{HAp})^{-1}[\langle S\rangle - f_2(\langle S\rangle - I)]^{-1} - I\}^{-1}T^{-T} + T^{-T}\}C_{M2}^{-1}\sigma_{M1}$$

or, expressed more simply

$$\sigma_{M1} = K_{aligned}\langle\varepsilon\rangle^{HAp}_{aligned}, \tag{5}$$

where $\langle C\rangle_{HAp}$ and $\langle S\rangle$ are the average stiffness and Eshelby tensor of HAp crystals in the gauge volume [44], C_{M2} is the collagen stiffness, and f_2 is the volume fraction of HAp with respect to the whole second-level structure. For perfectly aligned crystals, $\langle C\rangle_{HAp}$ and $\langle S\rangle$ can be represented by the value of a single crystal $\langle C\rangle_{HAp} = C_{HAp}$, $\langle S\rangle = S$. Note that different orientations (different transformation matrices) may result in different results of $\langle\varepsilon\rangle^{HAp}_{aligned}$. The variation of $K_{aligned}$ with different alignment angles of particles with respect to the loading direction can be calculated by changing the transformation matrix in Eq. (5).

3.3.2. Multiple randomly distributed HAp crystals

If HAp crystals have a random distribution, this group of crystals will have an isotropic stiffness, as well as an isotropic Eshelby tensor, and thus the relationship between the average local Hap crystal strain and external load is independent on the orientation matrix in Eq. (5):

$$\langle\varepsilon\rangle^{HAp}_{random} = \{\{(I - C_{M2}^{-1}\langle C\rangle_{HAp})^{-1}[\langle S\rangle - f_2(\langle S\rangle - I)]^{-1} - I\}^{-1} + I\}C_{M2}^{-1}\sigma_{M1}$$

or, expressed more simply

$$\sigma_{M1} = K_{random}\langle\varepsilon\rangle^{HAp}_{random}. \tag{6}$$

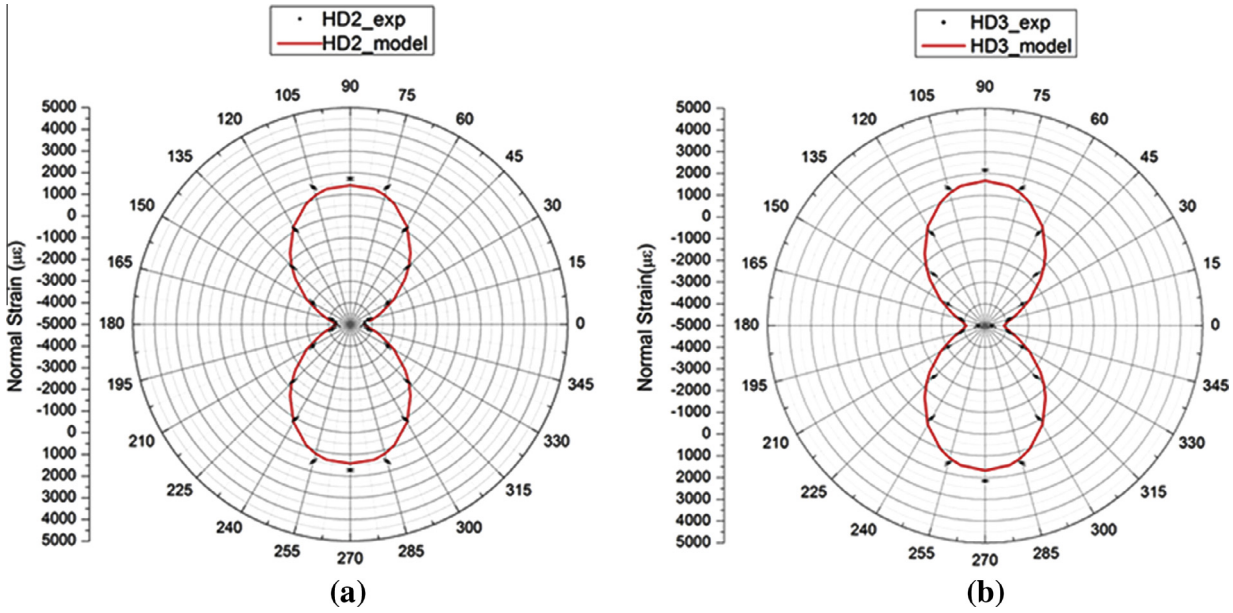

Fig. 5. Comparison of experimental data and modelling results of normal strain component variation with orientation distribution (0°–360°) under polar coordinates. (a) HD2 data (black points) and model fitting (red curve), with the compressive stress along transverse direction with respect to the tubules. (b) HD3 data (black points) and model fitting (red curve), with the compressive stress along the longitudinal direction with respect to the tubules.

In contrast to perfectly aligned crystals, $\langle S\rangle$ and $\langle C\rangle_{HAp}$ values were not those of the single crystal, but were obtained from the volume average of all the randomly distributed crystals (see Appendix, averaging the results obtained from each single-crystal relationship as Eq. (5) over all possible orientations).

3.3.3. Multiple HAp inclusions with partial alignment

In general, HAp crystals are partially aligned, thus $K^{HAp}_{partial\_aligned}$ is expected to be between K_{random} and $K_{aligned}$:

$$K^{HAp}_{partial\_aligned} = (1 - f_{aligned})K_{random} + f_{aligned}K_{aligned}, \quad (7)$$

where $f_{aligned}$ is the volume fraction of aligned crystals with respect to all HAp crystals, i.e. the degree of alignment of crystals revealed by SAXS measurements.

4. Experimental results and model validation

4.1. Nanoscale HAp distribution and mechanical response of dentine

The loading areas of the samples were accurately determined by micro-CT measurement. The loading areas were 4.466 mm^2 (HD2) and 4.413 mm^2 (HD3), respectively. Fig. 2a shows a WAXS pattern of dentine consisting of a system of Debye–Scherrer rings (peaks). The apparent radial shifts of the (002) peak in the WAXS pattern were measured under uniaxial compressive loading applied on both longitudinal and transverse directions with respect to the preferential tubule direction. Values of the shifts along the x-direction were used to obtain the elastic lattice strain variation along loading direction. Fig. 4a,b show the experimental results of the applied stress vs. HAp lattice strain of samples HD2 and HD3, indicating a linear increasing tendency as expected. The maximum load used in the model of the two samples was limited to ~100 MPa in the elastic region. The ratio of the uniaxial stress and the average HAp lattice strain gives the apparent modulus, which is listed in Table 1. From Fig. 4, it is observed that the dentine sample loaded along the longitudinal axis (HD3) has a slightly higher apparent modulus than the one loaded transversally (HD2). The residual (initial) strains were found to be quite small, namely, 205 $\mu\varepsilon$ (HD2) and −578.6 $\mu\varepsilon$ (HD3).

The (002) peak shifts along other directions were also measured by caking each pattern with a step of 20° (in the range of 0°–360°, Fig. 2a) to determine the normal strain component variation. The result is shown in polar coordinate as an azimuthal plot in Fig. 5a,b for HD2 and HD3, respectively, where 0° or 180° represents the loading direction and 90° or 360° represents that perpendicular to the loading direction. Being symmetrical, the results in the typical range of 0°–90° display a positive normal strain from 60°–90° and a negative normal strain from 0°–60°.

Fig. 2b is one of the SAXS patterns of the HD2 sample. The preferential orientation of HAp crystals is shown in the figure to be roughly along the short axis of the elliptical pattern. Fig. 2c is the plot of $I(\varphi)$ of the HD2 sample without any external load. The Gauss fit is also shown in the figure (red line). The detailed values of the orientation and degree of alignment were obtained by examining the plot of $I(\varphi)$ and are listed in Table 1. The degree of alignment values for both samples are relatively small, indicating that, as expected, the distribution of HAp crystals in human dentine is close to random, but nevertheless not entirely random.

4.2. Evaluation and testing of the multiscale Eshelby model

In the model, the material properties and other parameters were derived from the literature and were refined by fitting with the experimental data. It should be noted that a precise determination of the volume fraction of tubules in the first level is not available with commercial micro-CT systems, due to the polychromatic nature of the X-ray source and the limited resolution. Thus, the reported volume fraction of tubules between 3.6 and 10.2% was used [45]. The average mineral concentration (HAp volume fraction) has been reported to be between 30.5% and 44.4% in human third molars, with a decreasing gradient towards the pulp [46]. In general, a Young's modulus of 1 GPa and Poisson's ratio is 0.30 for collagen is given in the literature, without taking into account the viscoelasticity and viscoplasticity for human dentine [27,28]. Polycrystalline HAp has a high Young's modulus (40–117 GPa), whereas the Poisson's ratio is 0.27 [47]. However, these values of the HAp Young's modulus were all from a single perfect crystal. In biological mineralized composites such as dentine, imperfectly shaped

crystals are likely to exist, thus the high Young's modulus may induce an error by overestimation [7]. In accordance with Qin and Swain, 40 GPa was chosen here as a combination of the intertubular modulus (35.8 GPa) and peritubular modulus (66.76 GPa) in the respective volume fractions [27]. For the penny-shaped Eshelby tensor, only the ratio of radius and thickness (a_1/a_3) of the penny is needed [4,5]. All the parameters refined to obtain a best fitting are listed in Table 1, also with the reported values from the literature.

4.2.1. First-level model

The dentine matrix stress for the first level is only dependent on the volume fraction of tubules (see Eq. (4)). The same volume fraction of tubules was used for both samples, thus they have the same value of matrix stress, $\sigma_{M1} = 1.09\sigma^A$.

4.2.2. Second-level model

Based on the SAXS measurement of degree of alignment (Table 1), the apparent moduli for each sample can be obtained from Eq. (7) with the values listed in Table 1. A comparison of the stress–strain curve along the loading direction between the experiment and model evaluation is shown in Fig. 4c,d, where the Voigt and Reuss bound predictions are also given. It is found that the Eshelby model prediction lies between the two bound results and is closer to the experimental data, which also reflects the overestimation of the apparent modulus in previous investigation using the Voigt bound [7]. Meanwhile, the comparison of normal strain variation in the azimuthal plot is presented in Fig. 5a,b. Good agreement was also observed.

5. Discussion

This is the first time that the combined SAXS/WAXS technique has been used to capture the nanoscale structure and its influence on the macroscopic mechanical behaviour of human dentine. Moreover, it is important to emphasize that the study was conducted using penetrating radiation (synchrotron X-rays), i.e. a probe for bulk structure and strain analysis. Unlike the vast majority of studies that rely on surface characterisation (SEM, atomic force microscopy, nanoindentation, Raman, etc.), this ensures that the effects of sample preparation (e.g. cutting and storage) are minimal, since they typically affect depths not exceeding ~0.05 mm out of the total sample thickness of 2 mm.

5.1. Refined parameters by the Eshelby model

The parameters refined by the multiscale Eshelby model, listed in Table 1, lie within the range of the values reported in literature. This indicates that the model can be used to predict the nanoscale parameters which are hard to obtain by experiment. Of the five refined parameters, the three key parameters are two volume fractions and the Young's modulus of the HAp crystal. Among these three parameters, the Young's modulus exerts the most significant influence on the result. In the optimization process, the two volume fractions were initially fixed at approximate values, and the Young's modulus was refined within the range reported in the literature. The samples of dental tissue in this case were taken from teeth extracted from young patients. Consequently, the volume fraction of tubules was expected to be high, and was assumed to be 10% for both samples. For the same reasons, HAp crystals were assumed to have a low volume fraction (~40%). Other reasons for the small volume fraction of HAp crystals may include that the cubes were cut from a position near the pulp chamber where the volume fraction is relatively small [46], and the possible superficial demineralization effect of water storage [48]. Based on the above assumption about the two volume fractions, the refined Young's modulus of HAp crystal was found to be approximately 90 GPa. At this stage, other parameters were refined as well, although it was found that they only had a minor effect on the apparent modulus result. The influence of the thickness variation on the apparent modulus is found to be small. For a crystal thickness of 2 nm, the K_model is respectively 22.87 GPa (HD2) and 24.189 GPa (HD3), while the K_model is 23.15 GPa (HD2) and 24.62 GPa (HD3) at for a thickness of 4 nm. In order to get best fitting both along loading direction and for normal strain variation, 2 nm is the best refined parameter.

5.2. Residual strain

Indeed, a thin layer of initial residual strain may be induced at the sample surface during cutting using a low-speed diamond saw. However, as clarified above, the effect of this step on the overall measurement will not exceed 5% overall. Initial strain may also be associated with the natural growth process of the tooth. In any case, as shown in Section 4.1, the initial existing residual strain is quite small. Furthermore, our experiment only considered the elastic response. (This is reflected in the linearity of the experimental stress–strain curve, and is an underlying assumption for the Eshelby model.) The presence of initial strain amounts to an offset that does not affect such parameters as the apparent modulus. In conclusion, the low-level residual strain can be ignored in the present analysis, as it does not influence the elastic mechanical behaviour of the crystals.

5.3. Normal strain components variation

To characterize and validate the model of the strain components in different directions, the normal strain variation of the HAp crystals with respect to different azimuthal angles (0°–90°) is shown in Fig. 5. The ratio of the normal strain component at 90° to that at 0° (absolute value) for each sample is almost the Poisson's ratio of the HAp crystals, which is reasonable. Meanwhile, it should be noted that HAp crystals oriented at around 60° azimuthal angle exhibit no normal strain, i.e. no peak shift, which demonstrates that the HAp crystals at this corresponding position are subjected to pure shear stress. From the model, since the first-level dentine matrix stresses are the same for the two samples, the difference in the modulus as well as the normal strain component variation may result from different orientations and degrees of alignment of HAp crystals (observed and measured by SAXS).

5.4. HAp crystal distribution effects

The extended multiscale Eshelby model established in the present analysis is able to capture the relationship between the function of human dentine and its multiscale structure. Moreover, it is also capable of evaluating the effect of the nanoscale structure (e.g. HAp crystal distribution) on the macroscopic mechanical response, which was not included in earlier studies [7,20]. To demonstrate the detailed effect of crystal distribution on the apparent modulus, a schematic diagram of a 3-D model of perfectly aligned crystals is selected (Fig. 6a) with only one angle freedom φ around the z-axis. All aligned HAp crystals are initially oriented at a 90° angle to the platelet surface along the global y-direction, which represents the position of $\varphi = 0^{\circ}$. The variation of $K_{aligned}$ along the loading direction was calculated and visualized in Fig. 6b (only the result of HD2 is shown since both samples have similar results). The larger the value of $K_{aligned}$, the smaller the average lattice strain of HAp crystals will be under a certain value of external load, i.e. the stiffer the HAp crystals will be. It is found that the value of

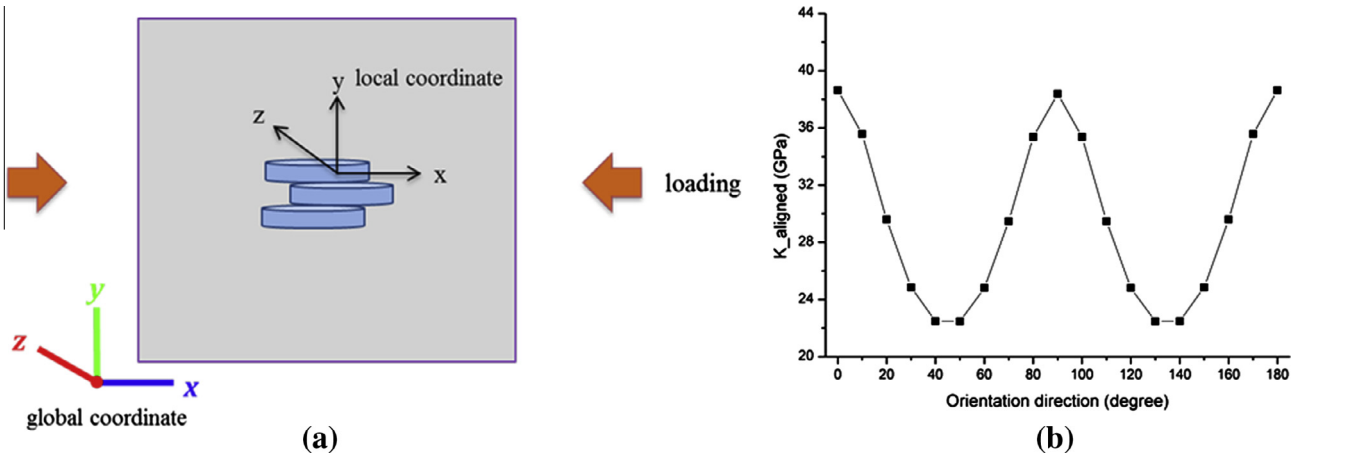

Fig. 6. (a) A simplified example of the alignment of HAp crystals. The beam direction is along the global z-axis and the alignment here represents the angle between the local x-axis and global x-axis (initially aligned angle $\varphi = 0^{\circ}$, i.e. the local x axis of a penny is initially along global x-axis). (b) By changing the alignment angle (0°–180°), the average strain of the crystals along loading direction can be obtained by the multiscale Eshelby model, which then indicates that $K_{aligned}$ varies with respect to the preferential alignment angle.

$K_{aligned}$ along the loading direction is strongly dependent on the crystal orientation direction. The orientations of HD2 and HD3 in our in situ loading experiments were 161° and 78°, respectively. Hence, from Fig. 6b, $K_{aligned\_HD3} > K_{aligned\_HD2}$. However, sample HD3 had a lower degree of alignment overall, so that overall the $K^{HAp}_{partial\_aligned\_HD3}$ value lies closer to K_{random}, which is the reason for the similar results of the apparent moduli of the two samples (Table 1).

6. Conclusions

In this study, the relationship between the nanoscale crystal distribution and macroscopic mechanical elastic response of human dentine was investigated for the first time using a combined in situ synchrotron SAXS/WAXS technique. This provided access to the information on both the structural and mechanical aspects of the sample that thus allowed us to make further progress compared to previous studies that only used WAXS [49]. Moreover, an extended multiscale Eshelby inclusion model was established to estimate and evaluate the elastic material properties of dentine as a two-level composite in terms of its constituents, showing good agreement with the experimental data both on lattice strain along loading direction and normal strain component in a general azimuthal plot, improving the Voigt composite model proposed earlier for bovine dentine [7]. The difference in the mechanical behaviour observed in the experimental results can be attributed to the second-level model effects, i.e. the degree of alignment and orientation angles.

Through this systematic experiment and modelling work, we are capable of observing the nanoscale structure, which is used to validate the model linking the nanoparticle arrangement and deformation behaviour to the macroscopic loading response. In addition, the parameter refinement and validation in the model adopted in the present study offers a possibility to identify the nanoscale parameters. The usual limitations of experimental characterization techniques such as nanoindentation or microscopy, e.g. confinement to the sample surface, make parameter identification difficult. We therefore argue that our approach enables the general characterization of the structure–property relationship in hierarchical biomaterials. An improved understanding of the multiscale structural–mechanical properties within human dentine is important for developing better prosthetic materials and dental fillings. It may also shed light on the mechanical property evolution due to multiscale structural changes within dentine because of disease and treatment.

Acknowledgements

A.M.K. acknowledges the support of EPSRC through grants EP/I020691 "Multi-disciplinary Centre for In-situ Processing Studies (CIPS)", EP/G004676 "Micromechanical Modelling and Experimentation", and EP/H003215 "New Dimensions of Engineering Science at Large Facilities". Diamond Light Source is acknowledged for providing the beam time.

Appendix A. Figures with essential colour discrimination

Certain figures in this article, particularly Figs. 1–6, are difficult to interpret in black and white. The full colour images can be found in the on-line version, at http://dx.doi.org/10.1016/j.actbio.2013.04.020

Appendix B. Appendix

A short overview of the Eshelby inclusion theory is given, leading to the derivation of the constitutive law for a non-dilute population of inhomogeneities (HAp crystals) embedded in a finite matrix.

B.1. Eshelby general theory

B.1.1. Dilute system

If a uniform transformation strain ε^{t*} exists in an ellipsoidal inclusion embedded in an infinite matrix, the Eshelby model shows that the total strain in the inclusion ε^{i} is related to ε^{t*} by the Eshelby tensor S that depends on the inclusion shape and Poisson's ratio:

$$\varepsilon^{i} = S\varepsilon^{t*}. \tag{B1}$$

Consequently, Hooke's law can be used to calculate the inclusion stress σ_I in terms of the elastic strain and the inclusion stiffness tensor C_M (which is the same as the surrounding isotropic matrix):

$$\sigma_I = C_M(\varepsilon^{i} - \varepsilon^{t*}) = C_M(S - I)\varepsilon^{t*}. \tag{B2}$$

If an inhomogeneity with a different stiffness tensor C_I is present, then the equivalent inclusion method can be used by considering the inhomogeneity as equivalent to an inclusion with an appropriate transformation strain ε^{t}, to be determined from the equivalence relation:

$$\sigma_I = C_I(\varepsilon^i - \varepsilon^{t*}) = C_M(\varepsilon^i - \varepsilon^t). \quad \text{(B3)}$$

If the material is subjected to an external load σ^A that results in the overall composite strain ε^A, then using Eq. (B3) the inclusion stress can be written as:

$$\sigma_I + \sigma^A = C_I(\varepsilon^i - \varepsilon^{t*} + \varepsilon^A) = C_M(\varepsilon^i - \varepsilon^t + \varepsilon^A). \quad \text{(B4)}$$

B.1.2. Non-dilute system

If multiple inhomogeneities are embedded in a finite matrix so that their volume fraction is not small, the composite is considered to be a non-dilute system. To satisfy the boundary conditions at the external boundaries of the finite composite, Eshelby introduced the concept of a mean "image" stress, $\langle\sigma\rangle_M = C_M\langle\varepsilon\rangle_M$ as an average of the stresses within individual phases, in order to maintain the balance of stress. The application of averaging to the linear Eq. (B4) gives:

$$C_M(\langle\varepsilon\rangle^i + \langle\varepsilon\rangle_M + \langle\varepsilon\rangle^A - \langle\varepsilon\rangle^t) = \langle C\rangle_I(\langle\varepsilon\rangle^i + \langle\varepsilon\rangle_M + \langle\varepsilon\rangle^A - \langle\varepsilon\rangle^{t*}), \quad \text{(B5)}$$

where $\langle C\rangle_I$ is the average stiffness of the inhomogeneities.

B.2. Dentine first-level model

The first-level model considers dentine as a composite consisting of aligned tubules within a finite matrix phase. According to Eq. (B5):

$$C_{M1}(\langle\varepsilon\rangle^i + \langle\varepsilon\rangle_{M1} + \varepsilon^A - \langle\varepsilon\rangle^t) = \langle C\rangle_{tubule}(\langle\varepsilon\rangle^i + \langle\varepsilon\rangle_{M1} + \varepsilon^A - \langle\varepsilon\rangle^{t*}), \quad \text{(B6)}$$

where $\langle C\rangle_{tubule}$ is the average stiffness of the tubules, and C_{M1} is the stiffness of the isotropic matrix or the equivalent inclusion ("*M1*" means the first-level matrix). Note that $\langle C\rangle_{tubule} = 0$ and $\langle\varepsilon\rangle^i = \langle S\rangle\langle\varepsilon\rangle^t$, thus:

$$\langle\varepsilon\rangle^t = (I - \langle S\rangle)^{-1}(\varepsilon^A + \langle\varepsilon\rangle_{M1}). \quad \text{(B7)}$$

In a non-dilute system, the mean image stress is related to the transformation strain [39] by:

$$\langle\sigma\rangle_{M1} = -f_1 C_{M1}(\langle S\rangle - I)\langle\varepsilon\rangle^t, \quad \text{(B8)}$$

where f_1 is the volume fraction of tubules with respect to the whole dentine. From Eq. (B7), considering that ($\langle\sigma\rangle_{M1} = C_{M1}\langle\varepsilon\rangle_{M1}$),

$$\langle\varepsilon\rangle_{M1} = \frac{f_1}{1 - f_1}\varepsilon^A. \quad \text{(B9)}$$

Therefore, the stress in the matrix is the sum of the applied stress and the image stress:

$$\sigma_{M1} = \sigma^A + \langle\sigma\rangle_{M1} = \frac{1}{1 - f_1}\sigma^A. \quad \text{(B10)}$$

Eq. (B10) indicates that the stress in the first-level matrix is independent on the direction and detailed shape (Eshelby tensor) of tubules.

B.3. Dentine second-level model

The second-level model considers the matrix of the first-level model to be a composite consisting of partially aligned HAp crystals and a collagen matrix. The volume-average method is introduced to determine the relationship between the external applied stress and the local averaged total strain in multiple HAp crystals.

The relationship between the strain in a single crystallite and the external stress can be established initially based on Eqs. (B1), (B2), (B3), (B4), (B5):

$$\begin{aligned}\varepsilon^{single} &= \{\{(I - C_{M2}^{-1}C_I)^{-1}[S - f_2(S - I)]^{-1} - I\}^{-1}T^{-T} \\ &\quad + T^{-T}\}C_{M2}^{-1}\sigma^A \\ &= K\sigma^A, \end{aligned} \quad \text{(B11)}$$

where "*M2*" means the second-level collagen matrix. C_I, S are the stiffness matrix and the Eshelby tensor for a single crystal, f_2 the volume fraction of HAp crystals with respect to the second-level composite and T is the orientation matrix described by three Euler angles (θ, ϕ, ψ). For a group of perfectly aligned HAp crystals, the relationship between the strain of the group and the external stress is the same as Eq. (B11), with the averaged stiffness and Eshelby tensor $\langle C\rangle_{HAp} = C_{HAp}, \langle S\rangle = S$. As for a group of randomly distributed HAp crystals, $\langle C\rangle_{HAp}, \langle S\rangle$ are isotropic and the way is to average the results of each single crystal (Eq. (B11)) within the group over all possible orientations:

$$\begin{aligned}\langle\varepsilon^{single}\rangle &= \frac{\int_0^{2\pi}\int_0^{\pi}\int_0^{2\pi} K\sin\theta d\phi d\theta d\psi}{\int_0^{2\pi}\int_0^{\pi}\int_0^{2\pi}\sin\theta d\phi d\theta d\psi}\sigma^A \\ &= \frac{\sigma^A}{2\pi^2}\int_0^{2\pi}\int_0^{\pi}\int_0^{2\pi} K\sin\theta d\phi d\theta d\psi = \langle K\rangle\sigma^A. \end{aligned} \quad \text{(B12)}$$

References

[1] Ten Cate AR, Dale AC. Oral histology: development, structure, and function. St. Louis, MO: Mosby; 1980.
[2] Petrovic LM, Spasic DT, Atanackovic TM. On a mathematical model of a human root dentin. Dent Mater 2005;21:125–8.
[3] Pashley DH, Ciucchi B, Sano H, Carvalho RM, Russell CM. Bond strength versus dentine structure: a modelling approach. Arch Oral Biol 1995;40:1109–18.
[4] Johansen E, Parks HF. Electron microscopic observations on the 3-dimensional morphology of apatite crystallites of human dentine and bone. J Biophys Biochem Cytol 1960;7:743–6.
[5] Voegel JC, Frank RM. Ultrastructural-study of apatite crystal dissolution in human dentin and bone. J Biol Buccale 1977;5:181–94.
[6] Kinney JH, Marshall SJ, Marshall GW. The mechanical properties of human dentin: a critical review and re-evaluation of the dental literature. Crit Rev Oral Biol Med 2003;14:13–29.
[7] Deymier-Black AC, Almer JD, Stock SR, Haeffner DR, Dunand DC. Synchrotron X-ray diffraction study of load partitioning during elastic deformation of bovine dentin. Acta Biomater 2010;6:2172–80.
[8] Deymier-Black AC, Almer JD, Stock SR, Dunand DC. Variability in the elastic properties of bovine dentin at multiple length scales. J Mech Behav Biomed Mater 2012;5:71–81.
[9] Young ML, Almer JD, Daymond MR, Haeffner DR, Dunand DC. Load partitioning between ferrite and cementite during elasto-plastic deformation of an ultrahigh-carbon steel. Acta Mater 2007;55:1999–2011.
[10] Mueller R, Rossoll A, Weber L, Bourke MAM, Dunand DC, Mortensen A. Tensile flow stress of ceramic particle-reinforced metal in the presence of particle cracking. Acta Mater 2008;56:4402–16.
[11] Young ML, DeFouw J, Almer JD, Dunand DC. Load partitioning during compressive loading of a Mg/MgB_2 composite. Acta Mater 2007;55:3467–78.
[12] Fratzl P, Schreiber S, Klaushofer K. Bone mineralization as studied by small-angle X-ray scattering. Connect Tissue Res 1996;35:9–16.
[13] Wagner HD, Weiner S. On the relationship between the microstructure of bone and its mechanical stiffness. J Biomech 1992;25:1311–20.
[14] Currey JD. The relationship between the stiffness and the mineral content of bone. J Biomech 1969;2:477–80.
[15] Bonfield W, Grynpas MD. Anisotropy of Youngs modulus of bone. Nature 1977;270:453–4.
[16] Deymier-Black AC, Yuan F, Singhal A, Almer JD, Brinson LC, Dunand DC. Evolution of load transfer between hydroxyapatite and collagen during creep deformation of bone. Acta Biomater 2012;8:253–61.
[17] Singhal A, Almer JD, Dunand DC. Variability in the nanoscale deformation of hydroxyapatite during compressive loading in bovine bone. Acta Biomater 2012;8:2747–58.
[18] Almer JD, Stock SR. Internal strains and stresses measured in cortical bone via high-energy X-ray diffraction. J Struct Biol 2005;152:14–27.
[19] Almer JD, Stock SR. Micromechanical response of mineral and collagen phases in bone. J Struct Biol 2007;157:365–70.
[20] Almer JD, Stock SR. High energy X-ray scattering quantification of in situ-loading-related strain gradients spanning the dentinoenamel junction (DEJ) in bovine tooth specimens. J Biomech 2010;43:2294–300.
[21] Lopes MB, Sinhoreti MA, Gonini Junior A, Consani S, McCabe JF. Comparative study of tubular diameter and quantity for human and bovine dentin at different depths. Braz Dent J 2009;20:279–83.
[22] Katz JL. Hard tissue as a composite material. 1. Bounds on elastic behavior. J Biomech 1971;93:455–73.

[23] Hashin Z. Analysis of composite-materials—a survey. J Appl Mech T Asme 1983;50:481–505.
[24] Gottesman T, Hashin Z. Analysis of viscoelastic behavior of bones on the basis of microstructure. J Biomech 1980;13:89–96.
[25] Withers PJ, Stobbs WM, Pedersen OB. The application of the Eshelby method of internal-stress determination to short fiber metal matrix composites. Acta Metall Mater 1989;37:3061–84.
[26] Takao Y, Taya M. The effect of variable fiber aspect ratio on the stiffness and thermal-expansion coefficients of a short fiber composite. J Compos Mater 1987;21:140–56.
[27] Qin Q-H, Swain MV. A micro-mechanics model of dentin mechanical properties. Biomaterials 2004;25:5081–90.
[28] Huo B. An inhomogeneous and anisotropic constitutive model of human dentin. J Biomech 2005;38:587–94.
[29] Wang YN, Qin QH. A generalized self consistent model for effective elastic moduli of human dentine. Compos Sci Technol 2007;67:1553–60.
[30] Huo B, Zheng QS. Effect of dentin tubules on the mechanical properties of dentin. Part I Stress–strain relations and strength criterion. Acta Mech Sin 1999;15:355–65.
[31] Diamond Light Source Calibration. 2013.
[32] Eliceiri KW, Berthold MR, Goldberg IG, Ibanez L, Manjunath BS, Martone ME, et al. Biological imaging software tools. Nat Methods 2012;9:697–710.
[33] Korsunsky AM, Baimpas N, Song X, Belnoue J, Hofmann F, Abbey B, et al. Strain tomography of polycrystalline zirconia dental prostheses by synchrotron X-ray diffraction. Acta Mater 2011;59:2501–13.
[34] Hammersley AP. FIT2D: an introduction and overview. ESRF Internal Report, 1997.
[35] Rinnerthaler S, Roschger P, Jakob HF, Nader A, Klaushofer K, Fratzl P. Scanning small angle X-ray scattering analysis of human bone sections. Calcified Tissue Int 1999;64:422–9.
[36] Tesch W, Vandenbos T, Roschgr P, Fratzl-Zelman N, Klaushofer K, Beertsen W, et al. Orientation of mineral crystallites and mineral density during skeletal development in mice deficient in tissue nonspecific alkaline phosphatase. J Bone Miner Res 2003;18:117–25.
[37] Tesch W, Eidelman N, Roschger P, Goldenberg F, Klaushofer K, Fratzl P. Graded microstructure and mechanical properties of human crown dentin. Calcified Tissue Int 2001;69:147–57.
[38] Bozec L, de Groot J, Odlyha M, Nicholls B, Nesbitt S, Flanagan A, et al. Atomic force microscopy of collagen structure in bone and dentine revealed by osteoclastic resorption. Ultramicroscopy 2005;105:79–89.
[39] Clyne TW, Withers PJ. An introduction to metal matrix composites. 1st pbk ed. Cambridge: Cambridge University Press; 1995.
[40] Mura T. Micromechanics of defects in solids. 2nd rev. ed. Dordrecht: Martinus Nijhoff; 1987.
[41] Stock SR, Veis A, Telser A, Cai Z. Near tubule and intertubular bovine dentin mapped at the 250 nm level. J Struct Biol 2011;176:203–11.
[42] Wenk HR, Heidelbach F. Crystal alignment of carbonated apatite in bone and calcified tendon: results from quantitative texture analysis. Bone 1999;24:361–9.
[43] Powers JM, Farah JW. Apparent modulus of elasticity of dental amalgams. J Dent Res 1975;54:902.
[44] Chou TW, Sun CT. In: Hyer MW, editor. Nanocomposites. DEStech Inc.; 2012.
[45] Dourda AO, Moule AJ, Young WG. A morphometric analysis of the cross-sectional area of dentine occupied by dentinal tubules in human third molar teeth. Int Endod J 1994;27:184–9.
[46] Kinney JH, Habelitz S, Marshall SJ, Marshall GW. The importance of intrafibrillar mineralization of collagen on the mechanical properties of dentin. J Dent Res 2003;82:957–61.
[47] Marten A, Fratzl P, Paris O, Zaslansky P. On the mineral in collagen of human crown dentine. Biomaterials 2010;31:5479–90.
[48] Habelitz S, Marshall Jr GW, Balooch M, Marshall SJ. Nanoindentation and storage of teeth. J Biomech 2002;35:995–8.
[49] Daniels JE, Pontoni D, Hoo RP, Honkimaki V. Simultaneous small- and wide-angle scattering at high X-ray energies. J Synchrotron Radiat 2010;17:473–8.